



# Along-strike variation of volcanic addition controlling post breakup sedimentary infill: Pelotas margin, Austral South Atlantic

Marlise C. Cassel<sup>1</sup>, Nick Kuszniir<sup>2</sup>, Gianreto Manatschal<sup>3</sup>, Daniel Sauter<sup>3</sup>

<sup>1</sup>Geological Institute / Organic Biochemistry in Geo-Systems Institute, RWTH Aachen University, Aachen, 52062, Germany

5 <sup>2</sup>School of Environmental Sciences, Liverpool University, Liverpool L69 3GP, UK

<sup>3</sup>Université de Strasbourg, CNRS, ITES UMR 7063, Strasbourg 67084, France

*Correspondence to:* Marlise C. Cassel (marlise.cassel@gmail.com)

**Abstract.** We investigate the lateral variability of breakup volcanic addition along-strike of the Pelotas segment of the Austral South Atlantic rifted margin and its control on post-rift accommodation space and sediment deposition. Our analysis of regional seismic reflection profiles shows that magmatic addition on the Pelotas margin varies substantially along strike from extremely magma-rich to magma-normal within a distance of ~300 km. Using 2D flexural backstripping we determine the post-rift accommodation space above top volcanics. In the north, where SDRs are thickest, the Torres High shows SDRs up to ~20 km thick and post-breakup water-loaded accommodation space is ~2 km. In contrast, in the south where magmatic addition is normal and SDRs are thinner, post-breakup water-loaded accommodation space is ~3 - 4 km. We show that post-breakup accommodation space correlates inversely with SDR thickness, being less for magma-rich margins and more for magma normal/intermediate margins. The Rio Grande Cone, with large sediment thickness, is underlain by small SDR thicknesses allowing large post-breakup accommodation space. A relationship is observed between the amount of volcanic material and the TWTT of first volcanics; first volcanics are observed at 1.25s TWTT for the highly magmatic Torres High profile while, in contrast, for the normally magmatic profiles in the south, first volcanics are observed at 4.2s TWTT or deeper. The observed inverse relationship between post-breakup accommodation space and SDR thickness is consistent with predictions by a simple isostatic model of continental lithosphere thinning and decompression melting during breakup.

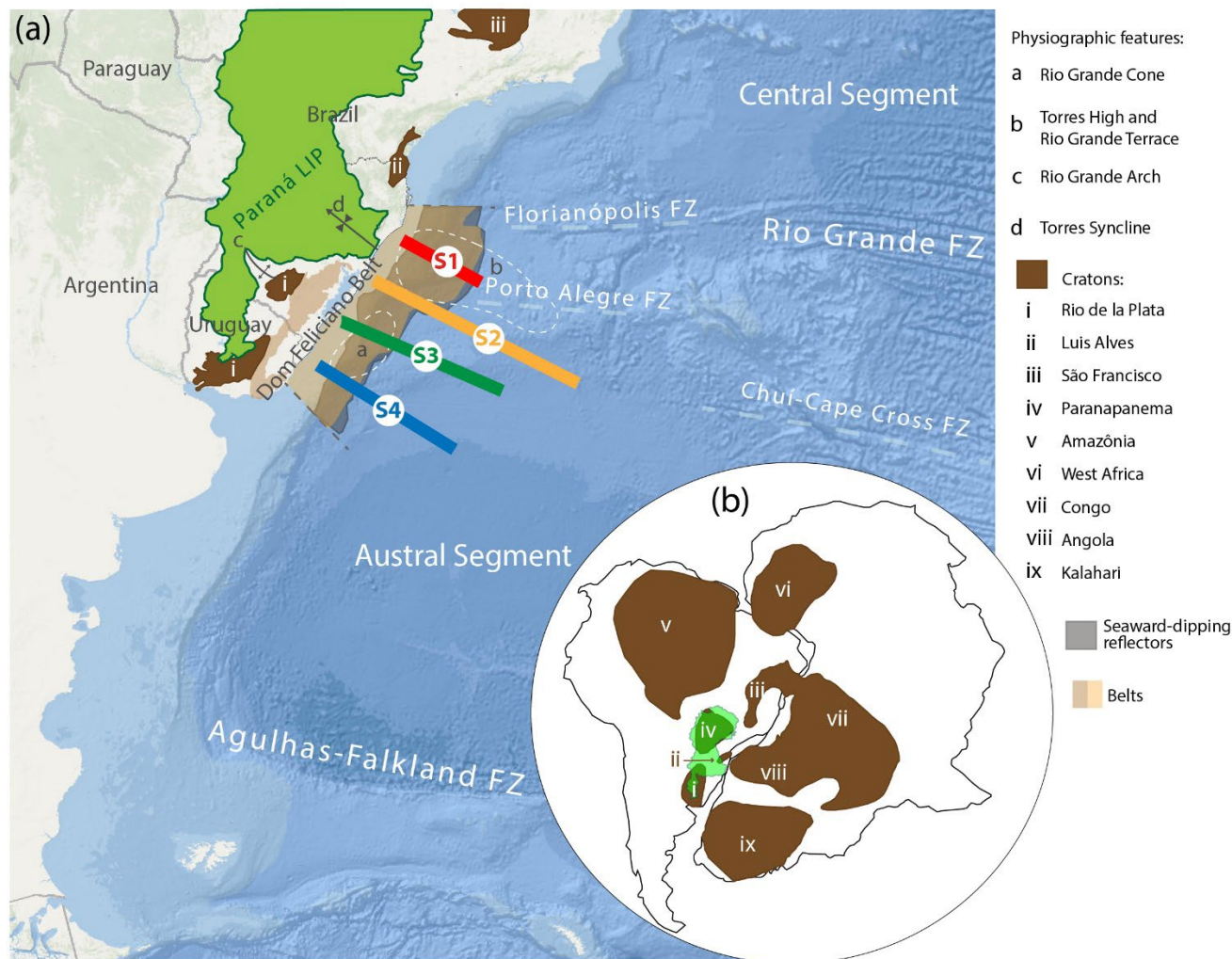
## 1 Introduction

In this paper we investigate lateral variability of breakup volcanic addition along-strike of the Pelotas segment of the Austral South Atlantic rifted margin and its control on post-rift accommodation space and sediment deposition. Breakup along the Austral segment of the S-Atlantic occurred by the propagation of rift systems accompanied by extensive magmatism, resulting in classical volcanic margins characterized by seaward-dipping reflectors (SDRs) (Koopman et al., 2014). While SDRs have been mapped and described in detail through dip sections along the Austral segment at both conjugate margins (Chauvet et al., 2021), much less is known about the along strike evolution of the magmatic system. Stica et al. (2014) and Franke et al. (2007) described the along strike evolution of the magmatic breakup, suggesting that the magmatic system was laterally continuous,



with breakup evolution being controlled by the Tristan mantle plume resulting in the Paraná-Etendeka magmatic province (Thompson et al., 2001; Peace et al. 2020). In contrast, a more recent study by Sauter et al. (2023) shows that the magmatic budget along large parts of the Austral segment does not need a hot-mantle booster and that higher magmatic budgets can only be observed north of the Chui-Cape Cross Fracture Zone when approaching the Paraná-Etendeka magmatic province. Sauter et al. (2023) analysed, however, only the magmatic budget recorded in the first oceanic crust. Important remaining questions are: do variations in magmatic addition occur along the Pelotas margin and, if variations do occur, how are they manifest in the margin architecture and how do they control margin accommodation space and depositional history.

Our study focuses on the Pelotas margin of the Austral South Atlantic located north of the Chui-Cape Cross Fracture Zone and offshore of the southeastern border of the Parana magmatic province (Fig. 1). We use four parallel deep long-offset seismic reflection dip lines that allow us to determine the along strike variation of volcanic thickness, sediment thickness and post-breakup accommodation space. We first examine the relationship between thicknesses of SDRs and sediments in two-way travel time (TWTT). We then use 2D flexural back-stripping of depth converted sections to determine post-rift accommodation space and its relationship with breakup volcanic addition. Our results reveal a direct relationship between the volume of breakup volcanics and post-breakup sedimentary fill along the Pelotas rifted margin. Our results contribute to the understanding of volcanic margins and their complex magmatic and sedimentary evolution.



50 **Figure 1: (a) Map of the Austral South Atlantic (adapted from Cassel et al., 2022) showing: the location of the 4 Pelotas Margin seismic reflection profiles examined in this study; the distribution of seaward-dipping reflectors from Chauvet et al. (2021); crustal basement from Stica et al. (2014); and Paraná Large Igneous Province (LIP) adapted from Rossetti et al. (2018). (b) Regional paleo-map of Western Gondwana adapted from Heilbron et al. (2008) showing the Paraná LIP and cratons.**

## 2 Geological setting

The Pelotas margin resulted from the assumed magma-rich breakup and separation of the Pangea super-continent during the Early Cretaceous. It is located offshore southern Brazil and is underlain by basement belonging to SW Gondwana. The continental basement is made of granitoids, schists and high-grade metamorphic rocks inherited from the Proterozoic Dom Feliciano Belt that records successive subduction and collision phases related to terrane accretion responsible for a strong NE-SW trending fabric. The overlying pre-breakup sedimentary succession was deposited in the intracratonic Paleozoic Paraná Basin, which is capped by a continental, fissural magmatism of the Paraná Large Igneous Province (Serra Geral Formation)

(Rossetti et al., 2018). These Lower Cretaceous flood basalts correspond to the Paraná-Etendeka Large Igneous Province that is tightly linked with the breakup of the Austral segment of the S-Atlantic (Zalan, 2004; Stica et al., 2014).

60 The Pelotas margin formed during the breakup of West Gondwana leading to the formation of the South Atlantic. This breakup may be regionally divided into Equatorial, Central and Austral segments with the Pelotas margin belonging to the latter (Stica et al. 2014). Stica et al. (2014) present a detailed compilation of the rift and breakup evolution of the Pelotas and conjugate Namibia margins. There is consensus that the Austral South Atlantic opening is diachronous, starting in the south and migrating northward (Franke et al., 2007). It is generally considered that final rifting and breakup of the Pelotas margin occurred in the  
65 Lower Cretaceous, with massive magmatic activity and the emplacement of high volumes of volcanic rocks forming prominent SDR sequences. The syn- to post-breakup sedimentary infill of the Pelotas margin can be subdivided into three main mega-sequences: i) transgressive mega-sequence (Aptian-Turonian), what includes the final rift phase, with depositional environments grading from continental deposits including alluvial conglomerates and lacustrine facies, to shallow marine evaporite, carbonate and siliciclastic facies deposited during breakup; ii) an aggradational mega-sequence (Turonian-  
70 Priabonian) with clastic fans in the more proximal domain and deeper marine shales and siltstone interbedded with turbiditic deposits in the distal domain; and iii) a regressive mega-sequence starting in Oligocene time and lasting to present, made of clastic fans and deltas that prograde oceanward over the distal deposits, forming a large regressive sedimentary wedge (Abreu and Anderson, 1998).

Recently, Cassel et al. (2022) demonstrated how along-strike variations in tectonic domains along the Andean convergence  
75 zone respond to the South Atlantic Mid Ocean Ridge spreading rate and control the margin evolution. While many of the previous studies have focused on the down dip and along strike magmatic evolution of the margin (Stica et al., 2014; Chauvet et al., 2021), little is known about the along-strike variations of the post-rift sediment accommodation and sediment-architecture and how it is linked to the volcanic addition. Here we focus on investigating the link between lateral variations of volcanic additions (e.g., SDR sequences) and the subsequent development of accommodation space and sedimentary infill  
80 along the Pelotas margin.

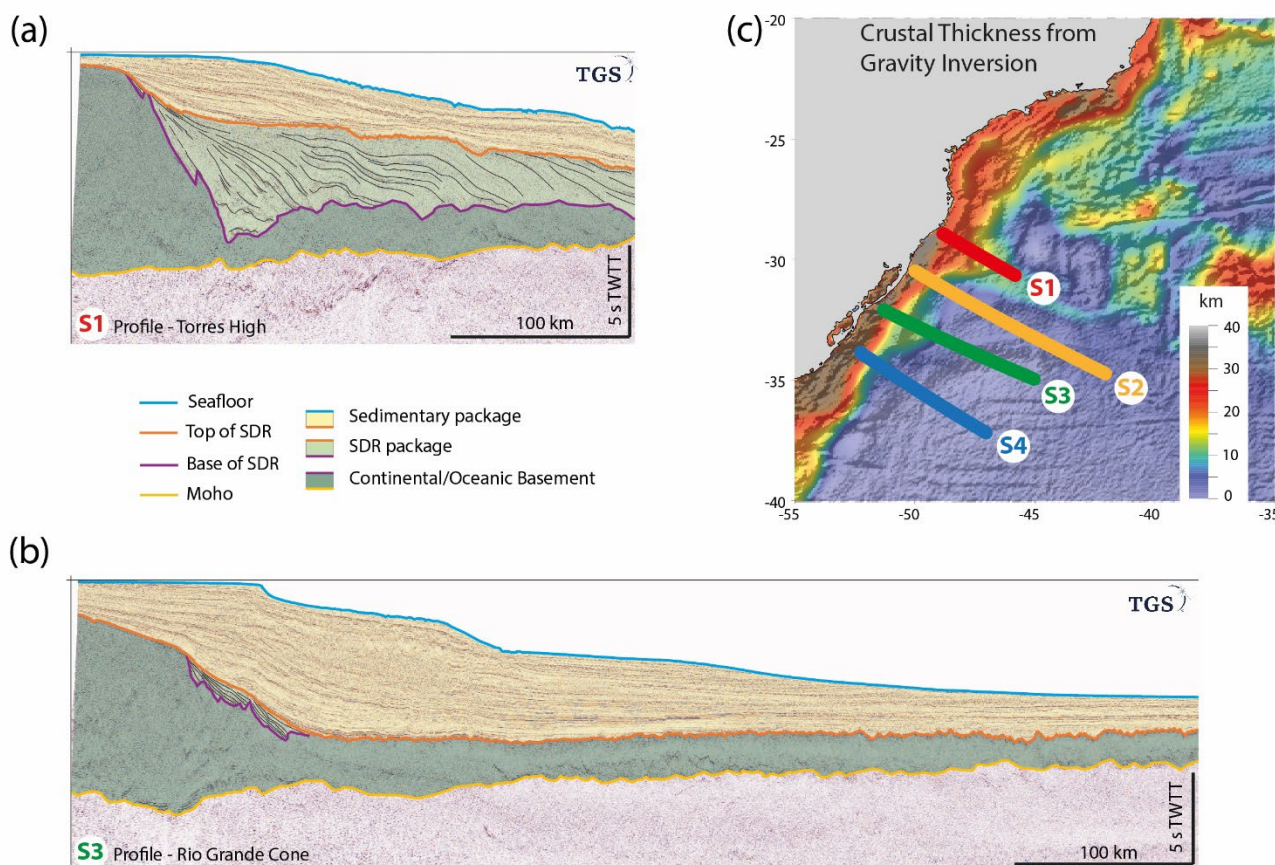
### 3 Along strike variation of volcanic addition and post-breakup sediment thickness

In this study, we interpret four parallel long-offset time-domain seismic reflection sections provided by TGS whose location is shown in Fig. 1. We identify three units in the seismic sections: a) continental/oceanic basement, b) volcanics (including SDRs), and c) sedimentary package. These units are bounded from top to bottom by the seafloor, top volcanics (including  
85 SDRs), base volcanics and Moho.

The basement unit is characterized by chaotic, discontinuous, low-amplitude reflectors (Fig. 2). Lines S1 and S3 (Fig. 2a and Fig. 2b) continentward of distance 100 km show that top continental basement tapers down to about 9s TWT. Oceanward of 100 km, top basement remains parallel to the distal end of the seismic sections. The top basement interface is a smooth horizon onto which the SDRs down-lap. The volcanic (SDR) package is characterized by several sequences of oceanward dipping,



90 oceanward diverging, high-amplitude reflectors. SDRs are well expressed on line S1, forming a thick volcanic package  
tapering oceanwards and overlying both the tapering and the box shaped basement. In contrast, for line S3, the SDRs are thin  
and overly only the crustal taper. The interface topping the SDR package corresponds to a sharp, high amplitude reflection  
interpreted to separate magmatic extrusives from the post-rift sedimentary package. The latter is well stratified, their reflectors  
95 have good lateral continuity and high frequency, showing parallel, sub-parallel, oblique and sigmoidal internal pattern,  
corresponding to progradational, aggradational and retrogradational depositional cycles previously described by Abreu and  
Anderson (1998).

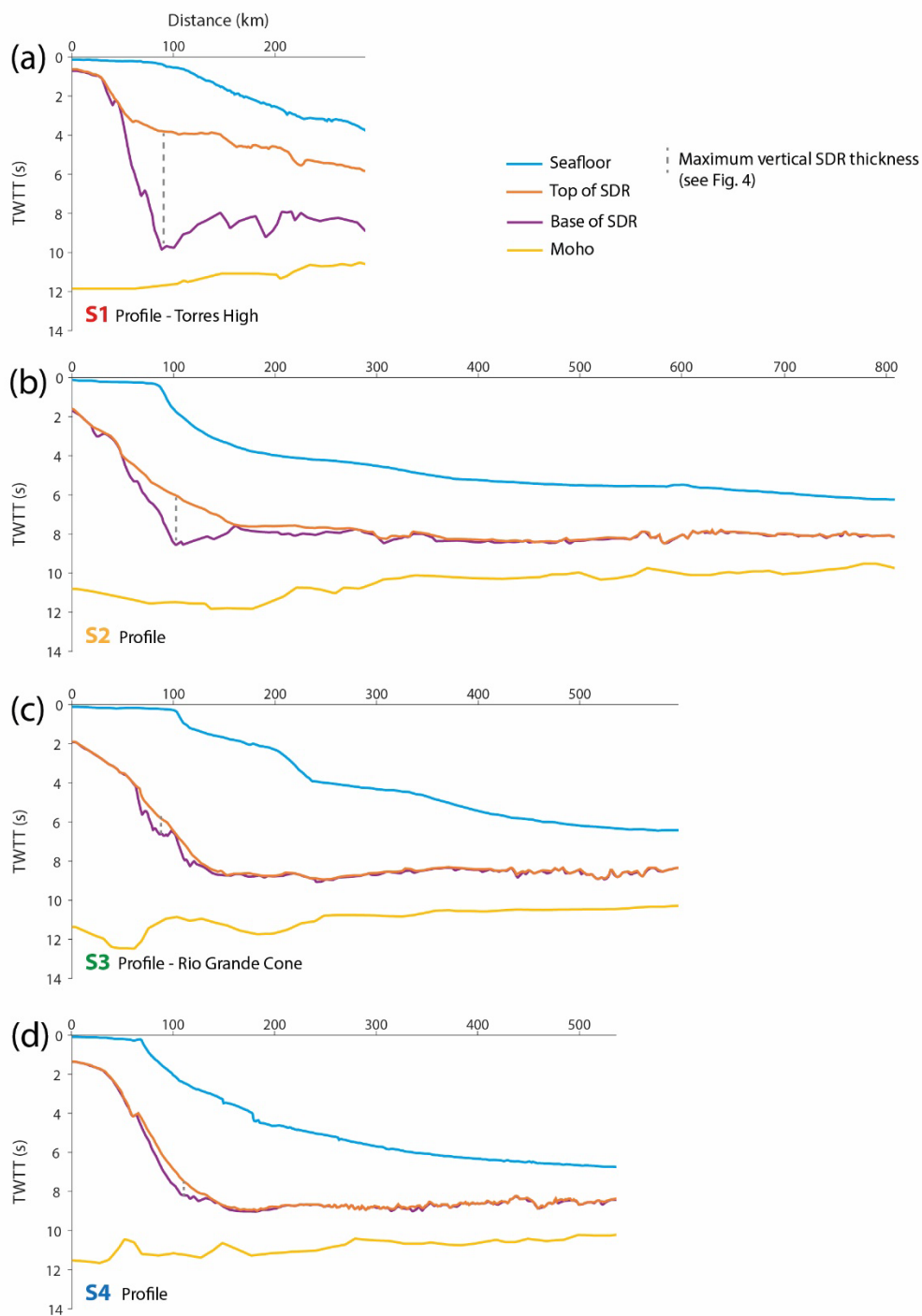


100 **Figure 2: (a) Seismic profiles in TWTT showing interpreted surfaces for profile S1 and S3: seafloor, top volcanics-SDRs, base volcanics and Moho. (b) Corresponding interpreted units for profile S1 and S3: continental/oceanic basement, volcanics-SDRs, and sedimentary packages. (c) Locations of the 4 seismic profiles superimposed on map of crust thickness from gravity inversion (adapted from Graca et al. 2019): Profile S1 is located in the northern Pelotas Basin along the Torres High. Profile S3 is located in the southern Pelotas Basin crossing the Rio Grande Cone.**

Comparison of the four seismic sections in a regional along-strike perspective (Fig. 3) shows some major differences. While  
105 in line S1 the continent ward termination of the SDR sequence starts at approximately 30 km at about 2s TWTT, in other  
sections the SDR package starts further oceanward at about 4 s TWTT (Fig. 3). The oceanward termination of the SDR  
package occurs, except for line S1, at the inflection point of top basement, i.e., at the change from a tapering to a box shaped

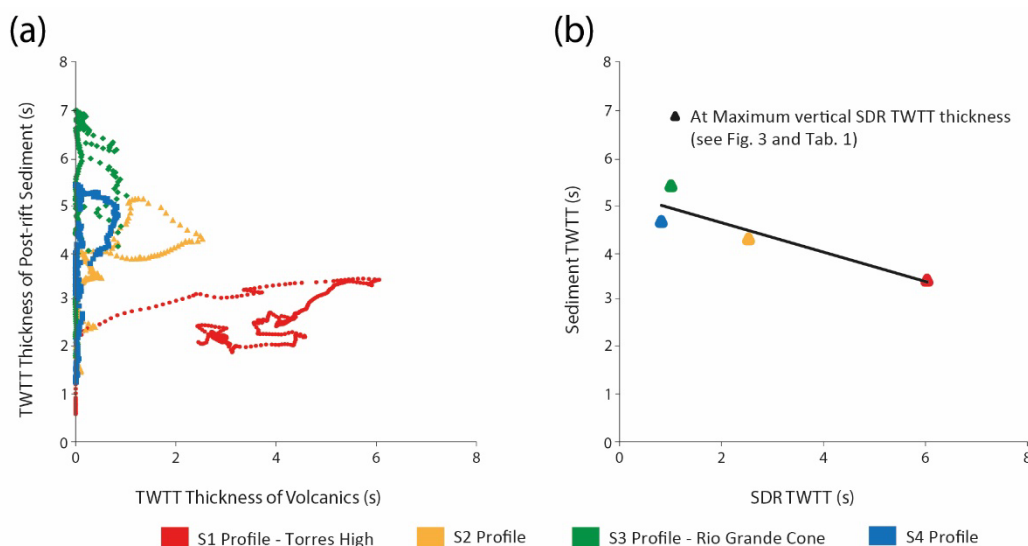


basement. Strong along-strike variations in the thickness of the volcanic (SDR) and sedimentary packages are shown in Table 1 and Fig. 4.





110 **Figure 3: Comparison of the 4 seismic profiles showing the interpreted surfaces in TWTT. (a) Seismic profile S1, located in the northern Pelotas Basin crossing the Torres High. (b) Seismic profile S2. (c) Seismic profile S3 located in the southern Pelotas Basin crossing the Rio Grande Cone. (d) Seismic profile S4.**



115 **Figure 4: (a) Plot of sediment thickness in TWTT against SDR thickness in TWTT at the same location out to profile distance 300 km for each of the 4 profiles S1-S4. (b) Plot of sediment thickness in TWTT against maximum SDR thickness TWTT at the same location for each profile S1-S4.**

**Table 1. Summary of vertical thickness measurements in TWTT taken from the Profiles S1 – S4, as shown in Fig. 3.**

| Profile | Maximum vertical thickness of SDR (s, TWTT) | Maximum vertical thickness of overlying sedimentary package (s, TWTT) | Ratio between vertical SDR and sediment thickness |
|---------|---|---|---|
| S1      | 6.06  | 3.80  | 1.59  |
| S2      | 2.53  | 4.00  | 0.62  |
| S3      | 1.01  | 6.00  | 0.16  |
| S4      | 0.84  | 5.80  | 0.14  |

120 Although all four seismic sections (S1-S4) show volcanic SDR packages, the thickness of volcanics and post-breakup  
 sediments show notable changes in vertical thickness along strike. Figure 4a shows a plot of vertical sediment thickness TWTT  
 against corresponding SDR thickness TWTT at the same horizontal distance for each profile out to 300 km distance. It shows  
 a clear difference between the value ranges of SDR and sediment thickness between the northern profile S1 (with high SDR  
 and low sediment thickness) and the southern profiles S3 and S4 (with low SDR and high sediment thickness). Profile S2  
 125 shows an intermediate relationship. The relationship between maximum SDR TWTT thickness and the corresponding sediment



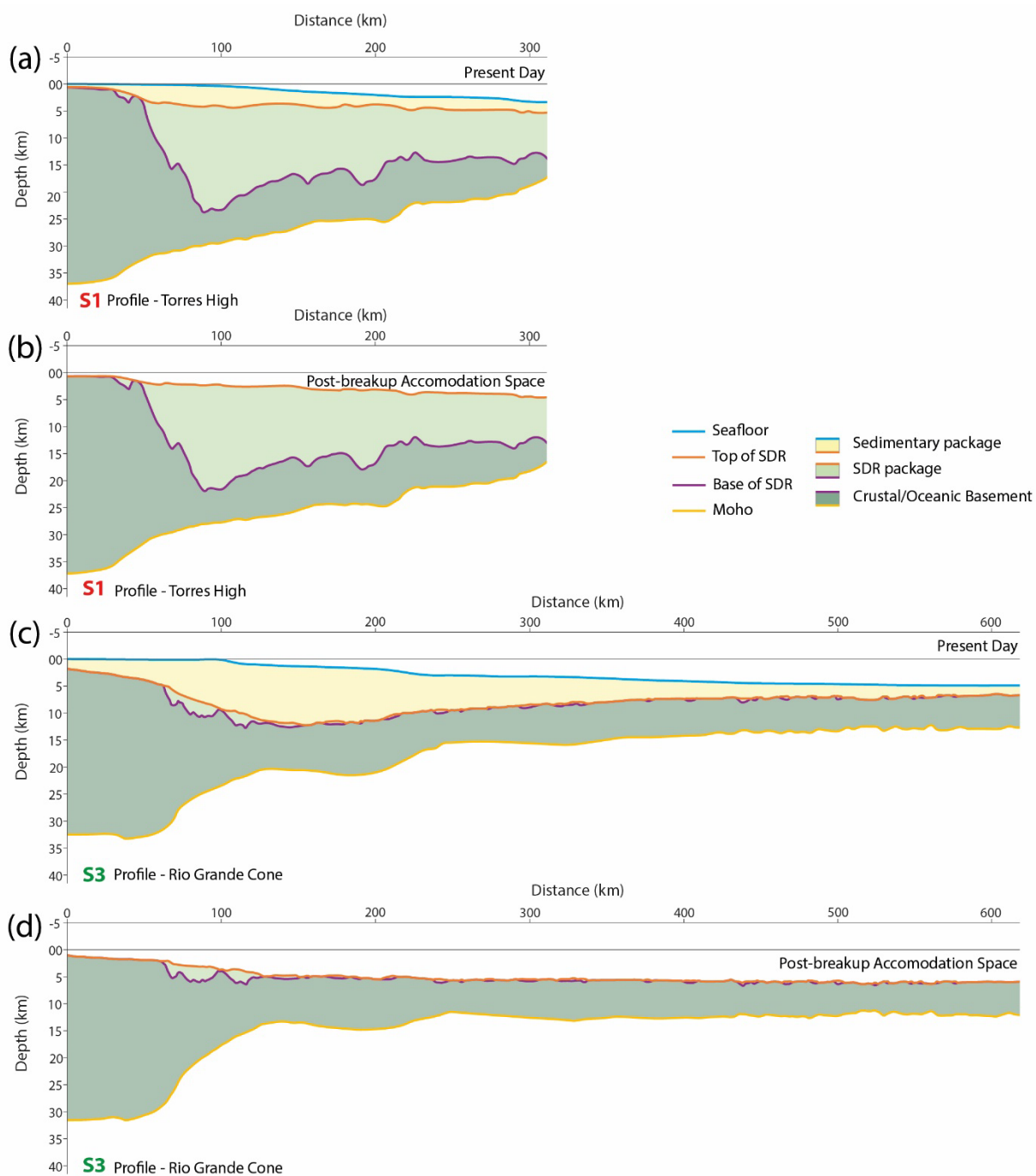
TWTT thickness at the same distance for each profile is shown in Fig. 4b. An inverse relationship can be seen; as volcanic (SDR) thickness in TWTT increases, the corresponding sediment TTWT decreases.

#### 4 Variation of post-breakup accommodation space and dependency on volcanic addition

In the previous section, we observed an inverse correlation of post-breakup sediment thickness with volcanic addition. However, margin sediment thickness is dependent on both sediment supply and accommodation space, sediment supply being controlled by factors external to margin formation. In this section we determine the post-rift accommodation space so that we can observe its relationship to volcanic addition.

Figures 5a and 5c show the depth converted seismic interpretations for the Torres High and the Rio Grande Cone profiles shown in Fig. 2. The depth conversion for post-rift sediment thickness uses a depth-dependent seismic velocity function  $V(z) = V_0 + k \cdot z$  where  $z$  is depth in km,  $V_0 = 1.75$  km/s and  $k = 0.4$  km/s<sup>2</sup>. Seismic velocities of SDRs range between 4.6 and 6.8 km/s (McDermott et al., 2019) depending on their composition. The SDRs of the Torres High profile are very thick and are most likely composed of basaltic flows. As a consequence, we use a higher velocity of 6.5 km/s for depth conversion. A sensitivity test using the lower value has been carried out and is discussed later. A seismic velocity of 6.5 km/s has been used for depth conversion of crustal basement (but has no influence on the determination of post-rift accommodation space).



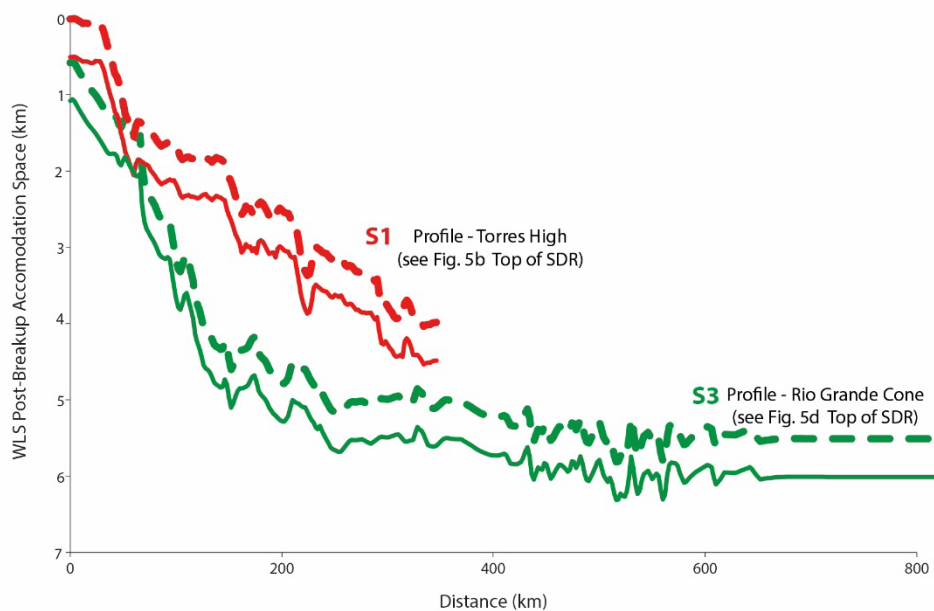


140

**Figure 5: (a and c) Comparison of present-day depth-converted sections S1 and S3 showing the interpreted surfaces of seafloor, top volcanics SDRs, base volcanics and Moho; and corresponding units of continental/oceanic basement, volcanics SDRs, and sedimentary package. (b and d) Comparison of water-loaded post-breakup accommodation space from flexural backstripping for profiles S1 and S3.**



- 145 Post-rift accommodation space has been determined from the depth converted sections using 2D flexural back-stripping. This process consists of calculating the isostatic load of sediments and the consequent isostatic lithosphere rebound resulting from removal of that load. This isostatic rebound is applied to the top basement depth to determine the bathymetry that would exist at present if no post-rift sedimentation had occurred. A detailed description of the 2D flexural backstripping methodology is given in Kuszniir et al. (1995) and Roberts et al. (1998). The magnitude of the sediment load depends on the thickness of
- 150 sediment and density increase with depth due to compaction. We assume that the post-rift sediments are normally pressured and have a shaly-sand lithology. Compaction parameters for a shaly-sand have been used (Sclater and Christie, 1980). The SDRs are assumed to have experienced negligible compaction. A  $T_e = 3\text{km}$  has been used to define the flexural strength of the lithosphere for the flexural back-stripping for removal of post-rift sediment loading (Roberts et al., 1998). Sensitivity tests to  $T_e$  are shown in Fig. S1.
- 155 The resulting water load accommodation space for the Torres High and Rio Grande Cone profiles are shown in Fig. 5b and Fig. 5d. These are directly compared in Fig. 6. For the same lateral position, the Rio Grande Cone profile shows significantly more accommodation space than the Torres High profile. While the predicted accommodation space is sensitive to the  $T_e$  value used in the flexural backstripping, the significant difference between accommodation post-rift space for S1 and S3 profiles remains.



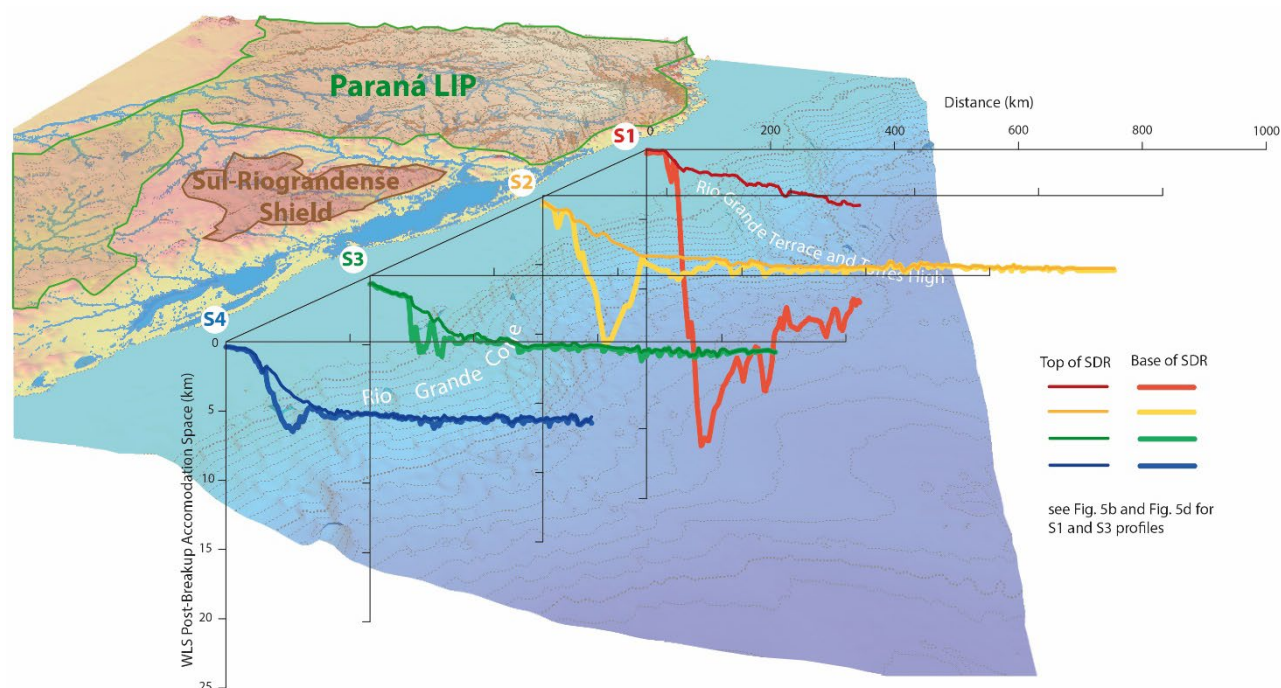
160

**Figure 6: Comparison of the water-loaded accommodation space from flexural backstripping (solid line) for the profiles S1 (Torres High) and S3 (Rio Grande Cone). Corresponding water-loaded accommodation space corrected for Oligo-Miocene dynamic subsidence (dashed line).**

- The southern South American continental margins, including the Pelotas segment, experienced significant subduction dynamic
- 165 subsidence in the Oligo-Miocene (Martinod et al., 2010; Shephard et al., 2012) A correction of 500m (a probable underestimate) decreases the component of post-rift accommodation space due to lithosphere thermal re-equilibration. This

component, directly related to the formation of the margin, when corrected for subduction dynamic subduction, is almost twice as large for the magma-normal southern profile (Rio Grande Cone) than the magma-rich northern profile (Torres High).

170 The along strike variation in post-rift accommodation space corrected for Oligo-Miocene subduction dynamic subsidence is shown in Fig. 7. Both Fig. 6 and Fig. 7 show that post-rift accommodation space increases substantially from north to south. This anti-correlation with the decrease in volcanic addition observed from north to south is shown in Fig. 3 and Fig. 4.



175 **Figure 7:** Comparison of water-loaded post-rift accommodation space for the 4 profiles S1-S4 showing north to south variation along the Pelotas Margin. Profiles S1 (Torres High) is offshore Serra Geral volcanics of the Parana LIP. Profiles S3 is offshore cratonic lithosphere of the Sul Riograndense Shield (SRS) where Serra Geral is absent.

## 5 Discussion

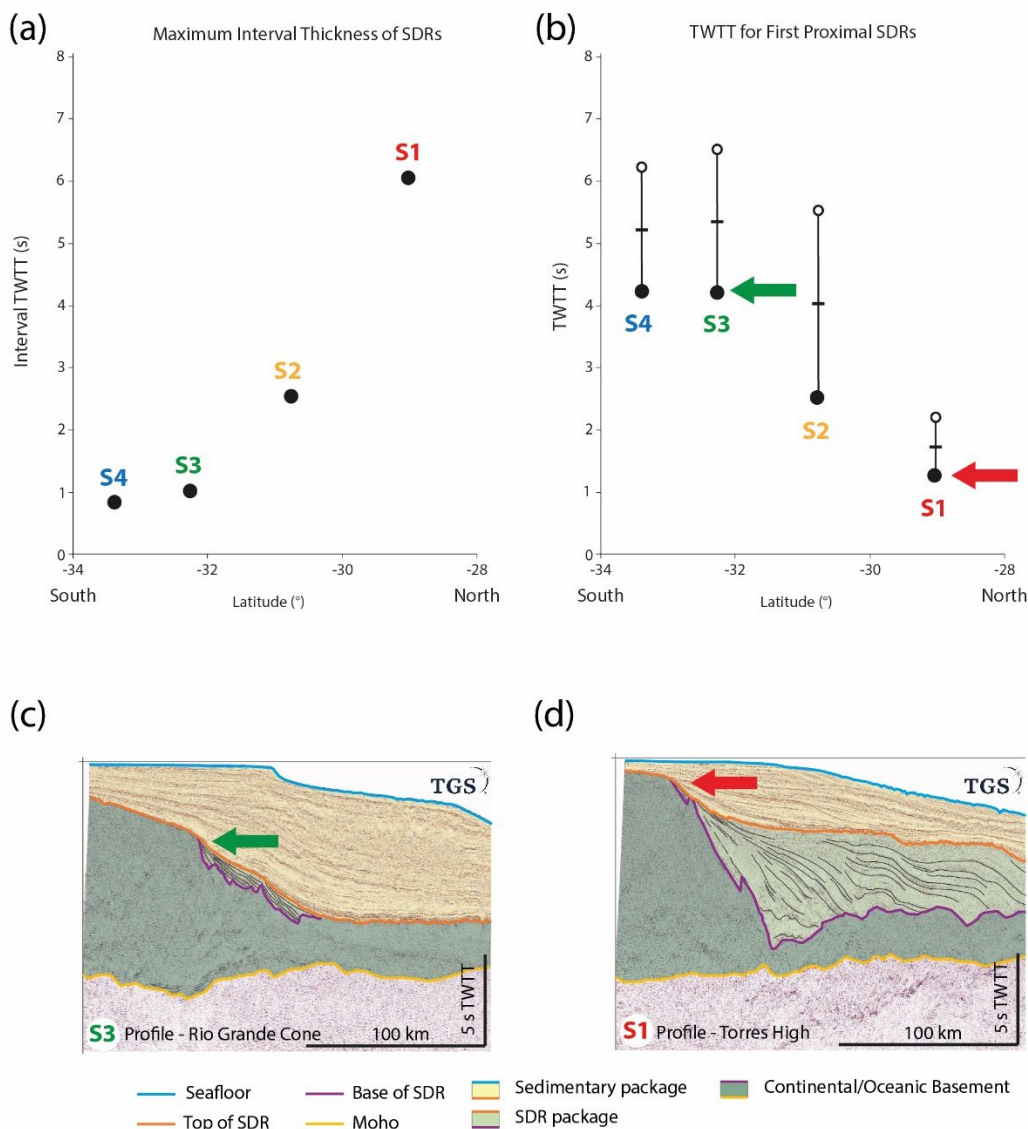
### 5.1 Along strike variation of magmatic addition along the Pelotas margin

180 The Austral segment of the South Atlantic margin of South American is often assumed to be magma-rich along its whole length, however our analysis of the seismic reflection sections 3 and 4 (Fig. 3) demonstrate that this is clearly not correct. While the northern profile S1 along the Torres High shows very large thicknesses of volcanic addition indicated by an up to 20 km thick SDRs package, the southern profiles S3 and S4 across the Central and South Pelotas margin segments display magmatic thicknesses more consistent with those of a normal margin with oceanic crustal thickness ~ 6.5 km (Bown and White, 1994; Dick et al., 2003).



185 Total magmatic addition on a rifted margin consists of the sum of magmatic intrusives emplaced within and at the base of  
thinned continental crust (often termed magmatic underplate) and volcanic extrusives. It is not possible to reliably quantify  
magmatic intrusives using seismic reflection and refraction data because their geophysical properties are similar to those of  
lower continental basement rocks (Karner et al., 2021). In our analysis we use the thicknesses of volcanic extrusives (SDRs in  
the case of profile S1) as a proxy for total magmatic volume. Estimates of the ratio of volcanic extrusives to magmatic  
intrusives/underplate range from approximately 1:2 for the Faeroes and Hatton Bank volcanic margins (White et al., 2008) to  
190 2:1 for the Demerara Plateau (Gomez-Romeu et al., 2022). In all cases, measured thicknesses of volcanic extrusives represent  
a lower bound of total magmatic volumes.

The north to south variation along strike of volcanic addition seen in Fig. 3 (in TWTT) and Fig. 7 (in depth) can be summarized  
by plotting maximum volcanic (SDR) interval TWTT against latitude. This north to south variation is shown in Fig. 8a and  
illustrates that the Pelotas margin is clearly not uniformly magma-rich. Within a distance of less than 300 km, volcanic addition  
195 varies from extremely magma-rich with SDRs up to 20km thick on the Torres High profile S1 to magma-normal for the Rio  
Grande Cone profile S3 in the south.



200 **Figure 8: (a) Maximum thickness of SDRs in TWTT for profiles S1-S4 plotted against latitude showing north to south decrease. (b) TWTT of first proximal occurrence of SDRs plotted against latitude showing north to south decrease. (c and d) Comparison of the seismic reflections sections for S3 and S1 in TWTT highlighting the first proximal occurrence of SDRs.**

This large variation in extrusive magmatic volumes along strike along the Pelotas margin is consistent with the observation reported in Sauter et al. (2023). This variation also correlates with the distribution of Serra Geral volcanics (Paraná LIP) on land (Fig. 1 Fig. and 7). Profiles 3 and 4, with normal magmatic volumes, are located offshore to where the Serra Geral is absent in Rio Grande do Sul. In contrast, profile S1, which shows the very large SDR thicknesses on the Torres High is located offshore where the Serra Geral is very thick and reaches the coast. The absence of Serra Geral in central and southern Rio Grande do Sul coincides with the presence of cratonic lithosphere of Sul Riograndense Shield (Chemale et al., 2021). In

205



contrast, on land to the north, the distribution of Serra Geral coincides with that of the Palaeozoic Parana Basin. As discussed in Sauter et al. (2023), this observed rapid decrease in magmatic volumes along strike may suggest that the large magmatic volumes observed in the north of the Pelotas margin (e.g., Torres High) are generated by a component of mantle inheritance rather than the usually assumed mantle-plume mechanism alone.

## 5.2 Along strike variation of accommodation space as consequence of magmatic addition

Examination of seismic reflection profiles S1-S4 indicates that there is an inverse correlation of sediment TWTT with SDR TWTT thickness (Fig. 3) as shown in the cross-plot in Fig. 4. Sediment thickness is controlled by many factors including source area erosion, sediment transport, deposition and preservation. As a consequence, we prefer to examine the lateral along strike variation in accommodation space rather than sediment thickness. Post-rift (post-SDR) accommodation space, determined using 2D flexural backstripping, shows large variations along strike (Fig. 5, Fig. 6 and Fig. 7), which inversely correlates with the thickness of extrusive volcanics.

During rifting leading to continental breakup, syn-rift subsidence occurs in response to thinning of the continental crust, which is partly offset by thermal uplift from geotherm elevation (McKenzie, 1978). After breakup, re-equilibration of the elevated geotherm results in post-rift thermal subsidence. The amount of accommodation space available for post-rift sedimentation depends on the sum of accommodation space generated by post-rift thermal subsidence and that remaining unfilled from the syn-rift stage.

In the north of the Pelotas margin, where magmatic addition was very large, syn-rift accommodation space was filled by extrusive volcanics producing almost 20 km of SDRs on the Torres High (profile S1). These SDRs have long lateral flow lengths, which are interpreted to indicate that the top of the SDRs were deposited at or above sea-level. As a consequence, the accommodation space available for post-rift sedimentation observed today and shown in Fig. 5, Fig. 6 and Fig. 7 consists of only that generated by post-rift thermal subsidence. In contrast in the south of the Pelotas margin (profiles S3 and S4), where magmatic addition is much less, syn-rift accommodation space was underfilled providing an additional contribution to add to accommodation space generated by post-rift thermal subsidence. As a consequence, more accommodation space is available in the south of the Pelotas margin for sediment deposition above volcanic extrusives. The observed inverse correlation of accommodation space with the thickness of extrusive volcanics can therefore be explained by the control of residual syn-rift accommodation by the volume of extrusive volcanics. Put simply, syn-rift accommodation space filled by extrusive volcanics is no longer available for post-rift sedimentation.

The Pelotas margin has two major present-day offshore physiographic features; the Torres High in the north (imaged on profile S1) and the Rio Grande Cone in the south (imaged by profile S3). The former exists because of magma-rich breakup generating very thick SDRs, the latter is located where the breakup occurred with much less magmatic addition provided a larger amount of accommodation for thick post-rift sedimentation. Both physiographic features control oceanic drifts by deflecting ocean currents but themselves have different origins. The variation in magmatic addition along the Pelotas margin exerts a strong control on depositional environments.

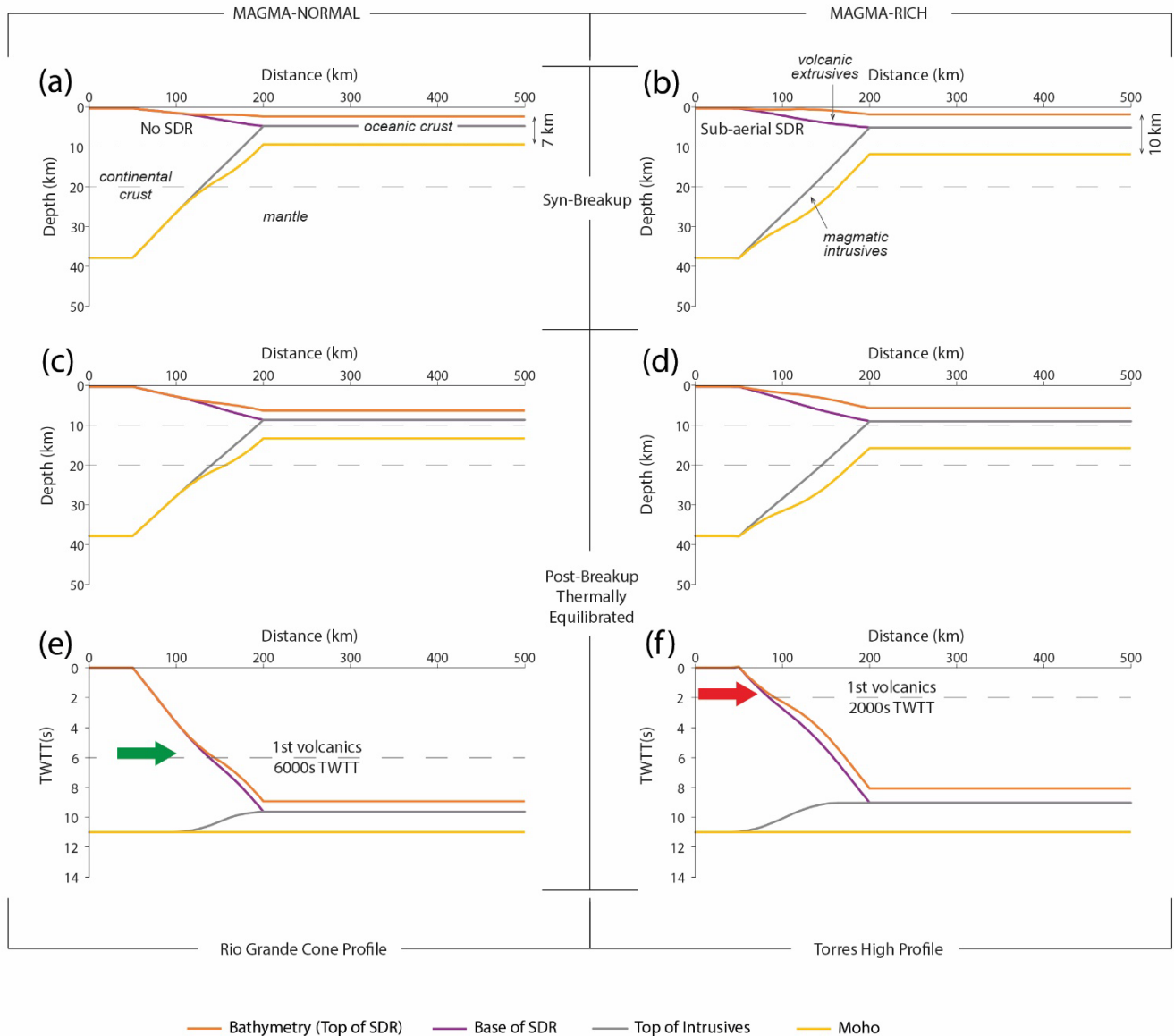


### 240 5.3 Significance of TWTT depth of first proximal volcanics on seismic reflection sections

Examination of the seismic reflection sections in the time domain shows that the TWTT for the first appearance of proximal SDRs is also very variable. For the magma-rich margin over the Torres High in the north, first volcanics occur at  $\sim 2$  s TWTT (Fig. 8d). In contrast, for the magma-normal margin profiles in the south, first proximal SDRs occur at 6 s or deeper (Fig. 8c). This north to south variation of TWTT of first volcanics is plotted as a function of latitude in Fig. 8b. The TWTT of first volcanic SDRs shows an inverse correlation with the magnitude of volcanic addition shown in Fig. 8a.

We explore this inverse correlation using a simple isostatically balanced model of a rifted margin with varying amounts of magmatic addition. The simple model, described in more detail in Chennin et al. (2023), calculates the isostatically balanced crustal cross-section for the idealised rifted margin produced by a prescribed crust and thinning taper showing resulting bathymetry, the remaining thickness of the continental crust and the thickness of new magmatic addition. The amount of decompression melt is calculated from the thinning factor taper using a parameterisation of the decompression melt model of White and McKenzie (1989). Isostatically balanced cross-sections are produced for thermally re-equilibrated lithosphere and at syn-breakup time by including lithosphere thermal uplift from the syn-tectonic elevated geotherm consistent with McKenzie (1978). Magmatic addition is partitioned 1/3 as extrusives overlying the thinned continental crust and 2/3 intrusives (underplate); in the oceanic domain these two layers correspond approximately to oceanic layers 2 and 3. The model is used to examine the magma-rich or magma-poor consequences for margin architecture and accommodation space resulting from increasing or decreasing the amount of decompression melt with respect to the 7 km generating normal oceanic crust and also the timing of melt initiation with respect to crustal thinning.

Figure 9 shows isostatically balanced margin cross-sections at breakup (with thermal uplift) and full thermal re-equilibration for an idealized margin with normal magmatic addition (left) and magma-rich addition (right). The magma-normal model assumes a maximum of 7 km magmatic addition (forming normal thickness oceanic crust) with decompression melting starting at  $\beta = 3$  consistent with the decompression melt model of White and McKenzie (1989). The magma-rich model has a maximum magmatic addition of 10 km (producing a 10km oceanic crust) with decompression melting starting at  $\beta = 2$  with the onset of decompression melting slightly advanced with respect to crustal thinning.



265 **Figure 9: Isostatically balanced model cross-sections of a rifted margin with varying amounts of magmatic addition. (a and b) at**  
**breakup time with syn-rift lithosphere thermal uplift. (c and d) at large post-breakup time with full lithosphere thermal re-**  
**equilibration. (e and f) Time domain representation of model cross-sections for full lithosphere thermal re-equilibration converted**  
**from depth model using Warner’s “10 second rule” (1987). The proximal onset of first volcanics is indicated by the coloured arrows.**  
 270 **Left column: an idealized margin with normal magmatic addition as for the Rio Grande Cone S3 Profile. Right column: an idealized**  
**magma-rich margin as for the Torres High S1 Profile.**

At breakup the magma-rich model shows (Fig. 9b) the upper surface of proximal volcanics at or above sea-level consistent with SDRs with long flow lengths as seen on the Torres High seismic section S1. In contrast the normal magmatic addition model shows (Fig. 9a) the upper surface of first volcanics at ~2 km water depth. The corresponding cross-sections after thermal re-equilibration and subsidence are shown in Fig. 9c and Fig. 9d.





275 Warner (1987) observed that the Moho TWTT on marine deep long-offset seismic data was at about 10 s TWTT for thermally  
equilibrated lithosphere and was remarkably constant (flat) in time irrespective of the complexity of the geology above  
including sediment thickness variation. Invoking Warner's 10 s rule for the Moho TWTT for thermally equilibrated lithosphere  
allows the cross-sections shown in Fig. 9c and Fig. 9d to be converted into the time domain as shown in Fig. 9e and Fig. 9f.  
In the time domain, first volcanics are predicted to occur at  $\sim 2$  s TWTT for the magma-rich model, while for the magma-  
280 normal magmatic addition model first volcanics occur at  $\sim 6$  s. These model predictions are consistent with the observations  
shown in Fig. 8.

## 6 Summary

- The amount of magmatic addition on the Pelotas margin varies substantially along strike from extremely magma-rich to magma-normal within a distance of  $\sim 300$  km.
- 285 • In the north, the Torres High shows SDR thicknesses of  $\sim 20$  km, and where the SDR package is thickest, post-breakup water-loaded accommodation space is  $\sim 2$  km
- In contrast, in the south, magmatic addition is normal, SDR thicknesses are small and where the SDR package is thickest, post-breakup water-loaded accommodation space is  $\sim 3 - 4$  km.
- Post-breakup accommodation space correlates inversely with SDR thickness, being less for magma-rich margins and  
290 more for magma normal/intermediate margins.
- The Rio Grande Cone, with large sediment thickness, is underlain by small SDR thicknesses allowing large post-breakup accommodation space.
- The observed inverse relationship between post-breakup accommodation space and SDR thickness is predicted by a simple isostatic model of continental lithosphere thinning and decompression melting during breakup.
- 295 • In the time domain, a magma-rich margin, with sub-aerial SDR flows, shows first volcanics at  $\sim 2$  s TWTT while a "normal" magmatic margin has first volcanics at 6 -7s TWTT.
- Our study shows that SDRs are not synonymous of magma-rich margins; the TWTT of first volcanics may provide a better approach to distinguishing magma-rich margins from margins with normal magmatic addition.

## Acknowledgements

300 We thank TGS for the seismic data supporting this study. The raw data are the private properties of TGSTM who should be contacted for any lending or acquisition ([https:// www.tgs.com/](https://www.tgs.com/)). We also thank colleagues to comments and discussion.



## References

- Abreu, V.S., and Anderson, J.B.: Glacial eustasy during the Cenozoic: sequence stratigraphic implications, *AAPG Bull.*, 82, 1385-1400, <https://doi.org/10.1306/1D9BCA89-172D-11D7-8645000102C1865D>, 1998.
- 305 Bown, J.W., and White, R.S.: Variation with spreading rate of oceanic crustal thickness and geochemistry. *Ear. Plan. Sci. Lett.*, 121, 435-449, [https://doi.org/10.1016/0012-821X\(94\)90082-5](https://doi.org/10.1016/0012-821X(94)90082-5), 1994.
- Cassel, M.C., Chemale Jr, F., Vargas, M.R., Souza, M.K., Girelli, T.J. and Oliveira, G.S.: From the Andes and the Drake Passage to the Rio Grande Submarine Fan: paleoclimatic and paleogeographic evidence in the Cenozoic Era from the South Atlantic – Austral Segment, Pelotas Basin, *Glob. Plan. Chan.*, 213, 103838, <https://doi.org/10.1016/j.gloplacha.2022.103838>,  
310 2022.
- Chauvet, F., Sapin, F., Geoffroy, L., Ringenbach, J.C. and Ferry, J.N.: Conjugate volcanic passive margins in the austral segment of the South Atlantic – Architecture and development, *Ear. Sci. Rev.*, 212, 103461, <https://doi.org/10.1016/j.earscirev.2020.103461>, 2021.
- Chemale, F., Lavina, E.L.C., Carassai, J.J., Girelli, T.J. and Lana, C.: Andean orogenic signature in the Quaternary sandy  
315 barriers of Southernmost Brazilian Passive margin – Paradigm as a source area, *Geosc. Fron.*, 12, 101119, <https://doi.org/10.1016/j.gsf.2020.11.015>, 2021.
- Chenin, P., Tomasi, S., Kuszniir, N. and Manatschal, G.: Linking Rifted Margin Crustal Shape with the Timing and Volume of Magmatism, *Terra Nova*, 0, 0-9, <https://doi.org/10.1111/ter.12690>, 2023.
- Dick, H.J.B., Lin, J. and Schouten, H.: An ultraslow-spreading class of ocean ridge, *Nature*, 426, 403-412,  
320 <https://doi.org/10.1038/nature02128>, 2003.
- Franke, D., Neben, S., Ladage, S., Schreckemberger, B. and Hinz, K.: Margin segmentation and volcano-tectonic architecture along the volcanic margin off Argentina/Uruguay, South Atlantic, *Mar. Geol.*, 244, 46-67, <https://doi.org/10.1016/j.margeo.2007.06.009>, 2007.
- Gomez-Romeu, J., Kuszniir, K., Ducoux, M., Jammes, S., Ball, P., Calassou, S. and Masini, E.: Formation of SDRs-Ocean  
325 transition at magma-rich rifted margins: Significance of a mantle seismic reflector at the western Demerara margin, *Tectonophysics*, 84520, 229624, <https://doi.org/10.1016/j.tecto.2022.22962>, 2022.
- Graca, M.C, Kuszniir, N. and Stanton, N.: Crustal thickness mapping of the central South Atlantic and the geodynamic development of the Rio Grande Rise and Walvis Ridge, *Mar. Petr. Geol.*, 101, 230-242, <https://doi.org/10.1016/j.marpetgeo.2018.12.011>, 2019.
- 330 Heilbron, M., Valeriano, C.M., Tassinari, C.C.G., Almeida, J., Tupinambá, M., Siga Jr., O. and Trouw, R.: Correlation of Neoproterozoic terranes between the Ribeira Belt, SE Brazil and its African counterpart: comparative tectonic evolution and open questions, in: *West Gondwana: Pre-cenozoic Correlations Across the South Atlantic Region*, edited by: Pankhurst, R.J., Trouw, R.A.J., Brito Neves, B.B. and De Wit, M.J., Special Publications, 294, Geological Society, London, 211-237, <https://doi.org/10.1144/SP294.12>, 2008.



- 335 Karner, G.D., Johnson, C., Shoffner, J., Lawson, M., Sullivan, M., Sitgreaves, J., McHarge, J., Stewart, J. and Figueredo, P.: Tectono-Magmatic Development of the Santos and Campos Basins, Offshore Brazil, in: *The Supergiant Lower Cretaceous Pre-Salt Petroleum Systems of the Santos Basin, Brazil*, edited by: Mello, M.R., Yilmaz, P.O. and Katz, B.J., AAPG Memoir, 124, AAPG, 215-256, 2021
- Koopmann, H., Brune, S., Franke, D. and Breuer, S.: Linking rift propagation barriers to excess magmatism at volcanic rifted  
340 margins, *Geol.*, 42, 1071-1074, <https://doi.org/10.1130/G36085.1>, 2014.
- Kusznir, N.J., Roberts, A. and Morley, C.: Forward and reverse modelling of rift basin formation, in: *Hydrocarbon Habitat in Rift Basins*, edited by: Lambiase, J., Special Publications, 80, Geological Society, London, 33-56, <https://doi.org/10.1144/GSL.SP.1995.080.01.02>, 1995.
- Martinod, J., Husson, L., Roperch, P. and Guillaume, B.: Horizontal subduction zones, convergence velocity and the building  
345 of the Andes, *Ear. Plan. Sci. Lett.*, 299, 299-309, <https://doi.org/10.1016/j.epsl.2010.09.010>, 2010.
- McDermott, C., Collier, J.S., Lonergan, L., Fruehn, J. and Bellingham, P.: Seismic velocity structure of seaward-dipping reflectors on the South American continental margin, *Ear. Plan. Sci. Lett.*, 521, 14-24, <https://doi.org/10.1016/j.epsl.2019.05.049>, 2019.
- McKenzie, D.P.: Some remarks on the development of sedimentary basins. *Ear. Plan. Sci. Lett.*, 40, 25-32,  
350 [https://doi.org/10.1016/0012-821X\(78\)90071-7](https://doi.org/10.1016/0012-821X(78)90071-7), 1978.
- Peace, A.L., Phethan, J.J.J., Frande, D., Foulger, G.R., Schiffer, C., Welford, J.K., McaHone, G., Rocchi, S., Schabel, M. and Doré, A.G.: A review of Pangaea dispersal and Large Igneous Provinces – In search of a causative mechanism, *Ear. Sci. Rev.*, 206, 102902, <https://doi.org/10.1016/j.earscirev.2019.102902>, 2020.
- Roberts A.M., Kusznir, N.J., Yielding G. and Styles P.: 2D flexural backstripping of extensional basins: the need for a sideways  
355 glance, *Petr. Geosc.*, 4, 327-338, <https://doi.org/10.1144/petgeo.4.4.327>, 1998.
- Sauter, D., Manatschal, G., Kusznir, N., Masquelet, C., Werner, P., Ulrich, M., Bellingham, P., Franke, D. and Autin, J.: Ignition of the southern Atlantic seafloor spreading machine without hot-mantle booster, *Sci. Rep.*, 13, 1195, <https://doi.org/10.1038/s41598-023-28364-y>, 2023.
- Sclater, J.G. and Christie, P.A F.: Continental Stretching: an explanation of the post mid-Cretaceous subsidence of the Central  
360 North Sea Basin, *Jour. Geoph. Res.*, 85, 3711-3739, <https://doi.org/10.1029/JB085iB07p03711>, 1980.
- Shephard, G.E., Liu, L., Müller, R.D. and Gurnis, M.: Dynamic topography and anomalously negative residual depth of the Argentine Basin, *Gond. Res.*, 22, 658-663, <https://doi.org/10.1016/j.gr.2011.12.005>, 2012.
- Stica, J.M., Zalán, P.V. and Ferrari, A.L.: The evolution of rifting on the volcanic margin of the Pelotas Basin and the contextualization of the Paraná-Etendeka LIP in the separation of Gondwana in the South Atlantic, *Mar. Petr. Geol.*, 50, 1-21,  
365 <https://doi.org/10.1016/j.marpetgeo.2013.10.015>, 2014.
- Rossetti, L., Lima, E.F., Waichel, B.L., Hole, M.J., Simoes, M.S. and Scherer, C.M.S.: Lithostratigraphy and volcanology of the Serra Geral Group, Paraná-Etendeka Igneous Province in Southern Brazil: Towards a formal stratigraphical framework, *Jour. Volc. Geoth. Res.*, 355, 98-114, <https://doi.org/10.1016/j.jvolgeores.2017.05.008>, 2018.



- Thompson, R.N., Gibson, S.A., Dickin, A.P. and Smith, P.M.: Early Cretaceous Basalt and Picrite Dykes of the Southern  
370 Etendeka Region, NW Namibia: Windows into the Role of the Tristan Mantle Plume in Paraná–Etendeka Magmatism, *Jour.  
Petr.*, 42, 2049–2081, <https://doi.org/10.1093/petrology/42.11.2049>, 2001.
- White, R.S. and McKenzie, D.: Magmatism at Rift Zones the Generation of Volcanic Continental Margins and Flood Basalts,  
*Jour. Geoph. Res.*, 94, 7685–7730, <https://doi.org/10.1029/JB094iB06p07685>, 1989.
- White, R.S., Smith, L.K., Roberts, A.W., Christie, P.A.F, Kuznir, N.J., Roberts, A.M., Healy, D., Spitzer, R., Chappell, A.,  
375 Eccles, J.D., Fletcher, R., Hurst, N., Lunnon, Z., Parkin, C.J. and Tymms, V.J.: Lower-crustal intrusion on the North Atlantic  
continental margin, *Nature*, 452, 460–464, <https://doi.org/10.1038/nature06687>, 2008.
- Zalán, P.V., 2004. Evolução Fanerozóica das Bacias Sedimentares Brasileiras. In: Mantesso-Neto, V., Bartorelli, A., Carneiro  
e, C.D.R., Brito-Neves, B.B. (Eds.), *Geologia do Continente Sul-Americano e Evolução da Obra de Fernando Flávio Marques  
de Almeida*. Beca Produções Culturais Ltda, São Paulo, pp. 595–612.